

Predictive Quantum Theory of Current and Optical Gain in Quantum Cascade Lasers¹

T. Kubis* and P. Vogl

Walter Schottky Institute, Technische Universität München, Am Coulombwall 3, 85748 Garching, Germany

*e-mail: Kubis@wsi.tum.de

Received November 12, 2008

Abstract—We have developed a flexible and accurate self consistent non-equilibrium Green’s functions method for stationary charge transport and optical gain in terahertz quantum cascade lasers. We compare our theoretical results with experimental data of a THz-QCL and find excellent quantitative agreement for the current-voltage characteristics and the peak gain energy. We identify non-radiative losses of electrons of the upper laser level to efficiently increase the threshold current and propose an optimized design that suppresses this coherent leakage.

PACS numbers: 73.23.-b; 72.20.-i; 78.67.Pt

DOI: 10.1134/S1054660X0904032X

1. INTRODUCTION

A realistic prediction of the performance of terahertz quantum cascade lasers (THz-QCLs) requires a theory of charge transport including coherent as well as incoherent effects. Since its development by Keldysh [1], Kadanoff and Baym [2] in the 1960’s, the non-equilibrium Green’s function theory (NEGF) has proven to be a reliable and accurate scheme for the calculation of quantum transport phenomena including scattering [3–11].

In the area of QCLs with its typically hundreds of unit cells, the NEGF method is most commonly applied in a basis of Wannier–Stark states that incorporate the electric field within this basis; this reduces the computational effort to a few QCL periods [9–11]. However, these schemes are restricted to strictly field periodic geometries and situations where (i) a combination of efficient scattering and high barriers limits the spatial extension of the electronic resonances, and (ii) no high energy carriers need to be taken into account. Since this approach lies outside the framework of scattering theory for open systems, current conservation cannot be obeyed rigorously.

The presently developed scheme is applicable to any type of open quantum device with attached leads where the carriers are in equilibrium. Both, the applied bias as well as the amount and type of coherent and incoherent scattering can be tuned from zero to infinity, or, in physical terms, from the ballistic to the diffusive limit. The formalism is based on scattering theory and guarantees exact current conservation. The state occupancies (represented by $G^<$) and electronic scattering states (G^R) are calculated self-consistently with one another which guarantees exact Pauli blocking. The nonlocal charac-

ter of the scattering self-energies due to phonons, impurities, interfaces are fully taken into account within the device as well as in the contact regions. The optical gain is calculated in linear response.

We apply our method to a class of THz-QCLs that have been successfully fabricated [12] and find excellent agreement between the calculated and observed current vs. voltage (I – V) characteristics, including the peak gain energy. The calculations indicate a significant coherent leakage of electrons of the upper laser level. We propose an optimized design for the QCL structures that suppresses this coherent leakage and significantly reduces the threshold current.

2. METHOD

All quantum cascade structures in this paper are GaAs/Al_{0.15}Ga_{0.85}As quantum well heterostructures that are homogeneous in the lateral x, y directions. They are assumed to be in contact with two equilibrium reservoirs at $z = 0$ and L . The electrons are described within a one-band model with a variable effective mass $m^*(z)$. We use the non-equilibrium Green’s function method (NEGF) to calculate stationary electronic transport and optical gain up to the threshold current in THz-QCLs. This method requires the solution of four coupled partial differential equations that read, in operator form,

$$(E - H_0 - e\Phi - \Sigma^R)G^R = 1, \\ G^< = G^R \Sigma^< G^{R\dagger}, \quad (1)$$

$$\Sigma^< = G^< D^<, \quad \Sigma^R = G^R D^R + G^R D^< + G^< D^R,$$

where H_0 is the single-electron Hamiltonian, Φ is the electrostatic potential, D is the sum of all environmental Green’s functions, and Σ denotes the self-energy. We

¹ The article is published in the original.

have implemented these expressions in a real space basis so that all Green's functions and self-energies are functions of two spatial coordinates z, z' , the lateral momentum k_{\parallel} , and the energy E . In this way, the scattering states, the transition probabilities between them and their occupations are calculated self-consistently. Once the Green's functions G^R and $G^<$ have been calculated, observables such as the current and the electron density can be calculated straightforwardly [3, 4].

We take into account inelastic acoustic and polar-optical phonon scattering, scattering by charged impurities, interface roughness, and by electron–electron interaction in the Hartree approximation. The full non-local momentum and energy dependence of the phonon, impurity and interface roughness self-energies are taken into account. We employ the self-consistent Born approximation for all scattering mechanisms in order to guarantee exact current conservation. Rough interfaces are described by a Gaussian in-plane roughness correlation with an autocorrelation length of 8 nm and a roughness step height of 0.6 nm, i.e., a roughness step height of ± 1 monolayer in growth direction. These values lie well within the range of typical experimental values for GaAs/AlAs interfaces [13–15]. All remaining material and transport parameters, such as electron-phonon and impurity interaction parameters have been taken from [16]. The electrostatic potential Φ is determined self-consistently with the Green's functions by solving the Poisson equation. We note that the condition of global charge neutrality only requires equal first derivatives of Φ at $z = 0$ and L . We determine the value for this derivative by the condition that the potential drop across the entire device matches the externally applied bias voltage.

We consider charge transport as a scattering problem from source to drain with the QCL structure as active device. In order to reduce the computational effort, the following procedure has proven to mimic faithfully the electronic and optical QCL properties. The two semi-infinite leads are assumed to consist of QCL periods, albeit with zero electric field and with the carriers obeying equilibrium Fermi statistics. The difference between the source and drain chemical potentials defines the applied bias voltage across the device. The electrons enter the device in propagating eigenstates of the respective infinitely extended lead Hamiltonians. The active device, where the applied bias drops and all the scattering occurs can then be restricted to a few QCL periods.

Our calculations show that for the type of THz QCLs considered in this paper, it actually suffices to treat a single QCL period as active device. In addition, even a flat band model for the leads (instead of multi quantum wells) yield virtually identical results for voltages up to the threshold voltage. This is a consequence of the high barriers within each QCL period that act as efficient energy filter so that the current does not

depend critically on the density of states of the incoming carriers [17].

We calculate the optical absorption coefficient in linear optical response, taking into account the calculated laser states and non-equilibrium state occupations, but we ignore vertex corrections to the self-energies. Banit et al. have shown [18] that the neglect of vertex corrections overestimates the emission line widths significantly. However, absorption peak positions and zeroes of the absorption coefficient seem to be much less sensitive to this approximation. We define the threshold voltage to be that voltage where the absorption coefficient at the peak gain energy (averaged over the active device) changes sign.

3. RESULTS

We have applied our method on carrier transport and optical gain within the active region of the terahertz GaAs/Al_{0.15}Ga_{0.85}As QCL structure of [12]. The geometry of this structure can be symbolically denoted by (30) 92 (55) 80 (27) 66 (41) 155. All quantities are given in angstroms, the values in parentheses indicate Al_{0.15}Ga_{0.85}As barrier widths, and the underlined value indicates the doped regions of the device. In this example, there is only a single n -doped well with $n = 1.25 \times 10^{16} \text{ cm}^{-3}$. It has been shown in the literature that the lattice temperature of a THz-QCL operated in pulsed mode increases by approximately 20–50 K above the heat sink temperature of 5 K [19, 20]. Therefore, we have set the temperature of the phonon bath and the contact reservoirs to 40 K.

3.1. Realistic Incoherent Transport

Incoherent scattering mechanisms are known to be crucial for the transport characteristics of QCLs [21]. Figure 1 shows a comparison of the measured (dots) and calculated (solid) I - V characteristics of the THz QCL of [12]. As can be seen from these results, our model excellently reproduces the experimental I - V characteristic. This suggests that the implementation of incoherent scattering with phonons, impurities and rough interfaces captures all relevant relaxation mechanisms.

Above the threshold voltage of approximately 46 mV, our model yields a negative differential resistivity, which originates from misaligned laser states. Since we do not include the coupling of the carriers to the laser field, the theoretical results underestimate the current density for voltages exceeding the threshold bias.

3.2. Coherent Leakage

A major portion of the total current stems from coherent transport, as can be deduced from the ballistic calculation depicted in Fig. 1. In fact, the ballistic current amounts to approximately 60% of the experimental

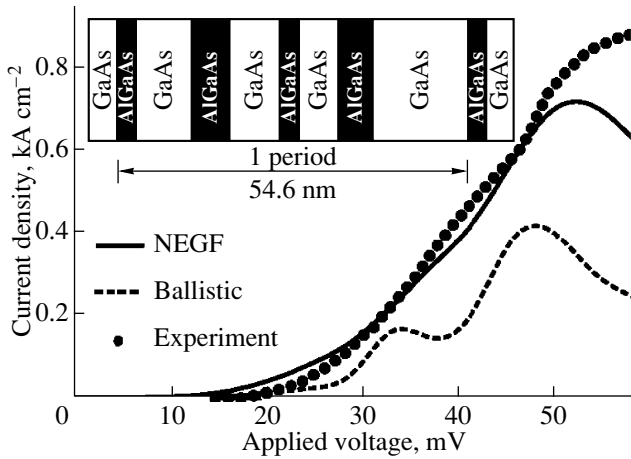


Fig. 1. Experimental (dots) and theoretically predicted (lines) I - V characteristics of the THz-QCL of [12]. Calculations that include all incoherent scattering mechanisms (solid) agree well with experiment. In contrast, purely coherent transport (dashed) can only partly reproduce the experiment. The inset shows the layer structure of a single period of the calculated device.

current near the threshold voltage. In order to further illustrate this result, Fig. 2 shows a contour plot of the energy and spatially resolved current density $j(z, E)$ close to the threshold voltage at 50 mV. The pronounced maximum of $j(z, E)$ in the energy windows from 0 and 30 meV extends over the entire QCL period. This implies that most of the electrons do not emit

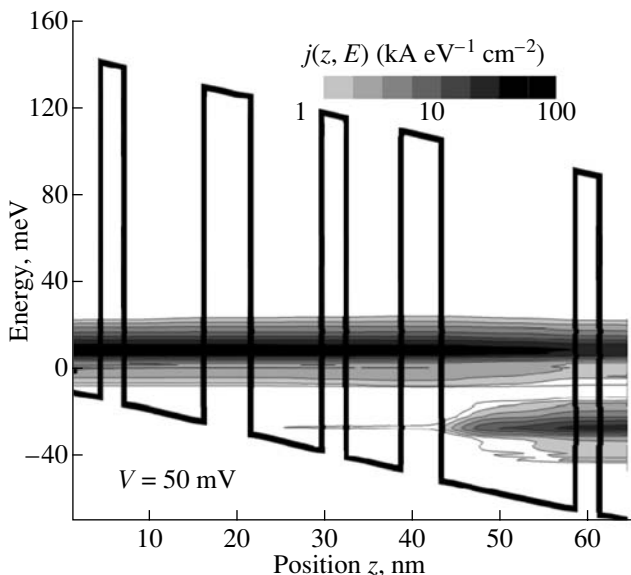


Fig. 2. Conduction band profile (solid line) and contour plot of the energy resolved current density $j(z, E)$ of the QCL in Fig. 1 close to threshold. The zero in energy marks the chemical potential of the source. A large portion of the propagating electrons crosses the QCL period without dissipating energy.

phonons until they reach the widest quantum well on the right hand side (around $z = 44$ nm). Figure 2 shows clearly that the amount of current carrying electrons at lower energies (about -25 meV) is rather small, considering the logarithmic scale in this graph.

In order to illustrate the mechanism that allows for this dissipationless transport, Fig. 3 depicts the energy and spatially resolved spectral function $A(z, E)$ of the QCL in Fig. 2 for vanishing lateral momentum $k_{\parallel} = 0$

$$A(z, E) = -i[G^R(z, z', 0, E) - G^{R\dagger}(z, z', 0, E)]. \quad (2)$$

The maxima of the spectral function represent resonant states. The dotted line in Fig. 3 shows the spectral function in the center of the QCL at $z = 36$ nm (see Fig. 2). The two peaks mark the lower ($E = -4$ meV) and the upper ($E = 9$ meV) laser level, respectively. The spectral function in the collector well ($z = 47$ nm in Fig. 2) is depicted by the solid line. It shows a resonance at the energy of the lower laser level. In addition, this collector state also overlaps with the upper laser level as can be deduced from the small peak that is marked by the arrow. In spite of being small, this overlap leads to a coherent leakage and reduces the occupation inversion. The electrons that are “lost” by this leakage leave the QCL cell with a net gain of kinetic energy.

3.3. Optimization with Suppressed Coherent Transport

The coherent leakage of the QCL structure discussed so far has several adverse effects for the device performance. It enhances the current density close to

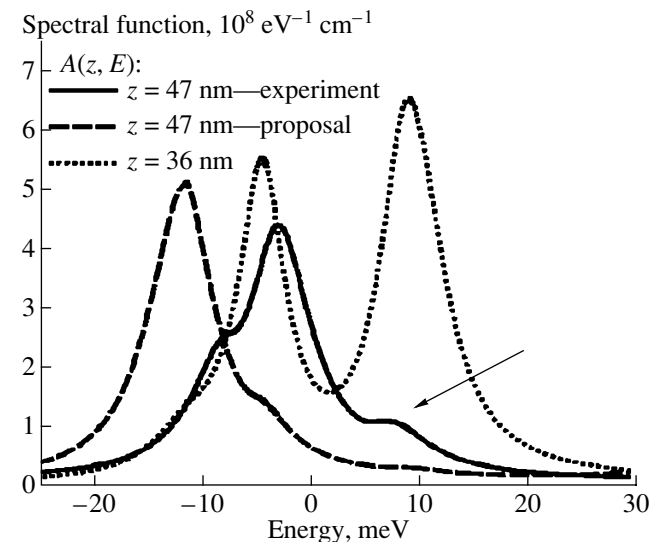


Fig. 3. Spectral function of the QCL in Fig. 2 as a function of energy E at different device positions. A resonance of the collector well of the experimental QCL (solid) overlaps with the upper laser level (dotted, at $E = 10$ meV) in the center of the QCL period (marked by the arrow). In the proposal, the collector well is broadened and this overlap is avoided (dashed).

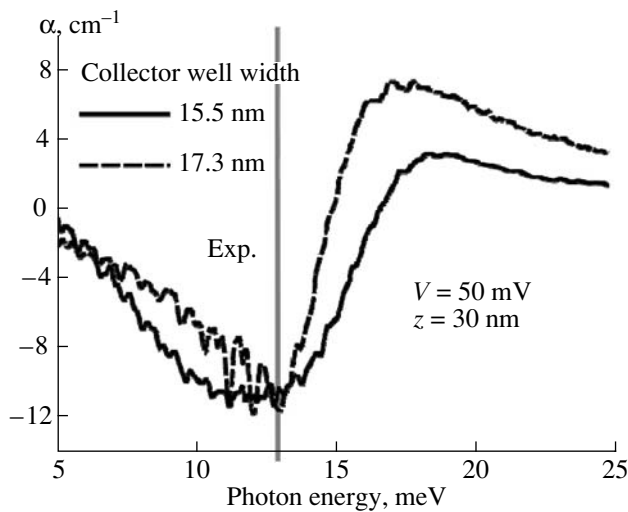


Fig. 4. Calculated absorption coefficient $\alpha(z, E_{\text{photon}})$ at the position $z = 30$ nm of the QCL in Fig. 2 (solid line) with a collector well width of 15.5 nm. The peak gain energy agrees with the experimental photon energy (grey line) and is not affected by the broadening of the collector well (dashed line).

threshold and causes a large number of electrons to tunnel out of the upper laser level without emitting photons. In order to suppress this leakage, the QCL should be designed in such a way that the upper laser level does not extend into the collector well. The simplest way to achieve this goal is to broaden the collector well since this automatically misaligns the collector well states with the laser levels. The dashed line in Fig. 3 shows the spectral function in the collector well for a collector well width of 17.3 nm (instead of 15.5 nm). With this design, the collector well state lies at lower energies and the spectral density in the collector well becomes very small at the energy of the upper laser level. This modification reduces the calculated current density at a bias of $V = 50$ mV per period from 0.70 to 0.59 kA/cm². It is important to note, that the present broadening of the collector well neither changes the peak gain energy nor the maximum value of the gain. This can be seen in Fig. 4, as it shows the optical absorption coefficient in the center of the experimental (solid) and the optimized QCL (dashed).

4. CONCLUSIONS

We have developed a self consistent non-equilibrium Green's function theory for stationary electron transport and optical gain in THz-QCLs. We consider the QCLs as open quantum devices. This allows one to include hot carrier effects and guarantees current conservation. Our model excellently reproduces the experimental I - V characteristics and the peak gain energy of the present THz-QCL. We find coherent and incoherent mechanisms to be equally important for the electronic

transport. In particular, coherent leakage of the upper laser level turns out to efficiently contribute to the threshold current. We propose an optimized design that efficiently suppresses this coherent leakage.

ACKNOWLEDGMENTS

The authors acknowledge financial support from the Deutsche Forschungsgemeinschaft (SFB 631), the Österreichische Fonds zur Förderung der Wissenschaft (SFB IRON), and the Nano Initiative Munich.

REFERENCES

1. L. P. Keldysh, Sov. Phys. JETP **20**, 1018 (1965)
2. L. P. Kadanoff and G. Baym, *Quantum Statistical Mechanics* (Benjamin, New York, 1962)
3. R. Lake, G. Klimeck, R. Bowen, and D. Jovanovic, J. Appl. Phys. **81**, 7845 (1997).
4. S. Datta, *Electronic Transport in Mesoscopic Systems* (Cambridge Univ., Cambridge, 1995).
5. M. P. Anantram and T. R. Govindan, Phys. Rev. B **58**, 4882 (1998)
6. A. Cresti, R. Farchioni, G. Grosso, and G. P. Parravicini, Phys. Rev. B **68**, 075306 (2003)
7. A. Svizhenko, M. P. Anantram, T. R. Govindan, B. Biegel and R. Venugopal, J. Appl. Phys. **91**, 2343 (2002)
8. A. Gagliardi, G. C. Solomon, A. Pecchia, T. Frauenheim, A. D. Carlo, N. S. Hush, and J. R. Reimers, Phys. Rev. B **75**, 174306 (2007).
9. A. Wacker, Phys. Rev. B **66**, 085326 (2002).
10. S.-C. Lee and A. Wacker, Phys. Rev. B **66**, 245314 (2002).
11. N. Vukmirović, Z. Ikonić, D. Indijin, and P. Harrison, Phys. Rev. B **76**, 245313 (2007).
12. A. Benz, G. Fasching, A. M. Andrews, M. Martl, K. Unterrainer, T. Roch, W. Schrenk, S. Golka, and G. Strasser, Appl. Phys. Lett. **90**, 101107 (2007).
13. B. R. Nag, Semicond. Sci. Technol. **19**, 162 (2004).
14. T. Unuma, M. Yoshita, T. Noda, H. Sakaki, and H. Akiyama, J. Appl. Phys. **93**, 1586 (2003).
15. K. Leosson, J. R. Jensen, W. Langbein, and J. M. Hvam, Phys. Rev. B **61**, 10322 (2000).
16. *Semiconductors: Intrinsic Properties of Group IV Elements and III-V, II-VI and I-VII Compounds*, Ed. by O. Madelung and Landolt-Börnstein, New Series, Group III/22 a (Springer, Berlin, 1987).
17. T. Kubis, C. Yeh, and P. Vogl, J. Comput. Electron. **7**, 432 (2008).
18. F. Banit, S.-C. Lee, A. Knorr, and A. Wacker, Appl. Phys. Lett. **86**, 041108 (2005).
19. M. Vitiello, G. Scamarcio, V. Spagnolo, B. S. Williams, S. Kumar, Q. Hu, and J. L. Reno, Appl. Phys. Lett. **86**, 111115 (2005).
20. H. Callebaut, S. Kumar, B. S. Williams, Q. Hu, and J. L. Reno, Appl. Phys. Lett. **83**, 207 (2003)
21. R. C. Iotti and F. Rossi, Phys. Rev. Lett. **87**, 146603 (2001).